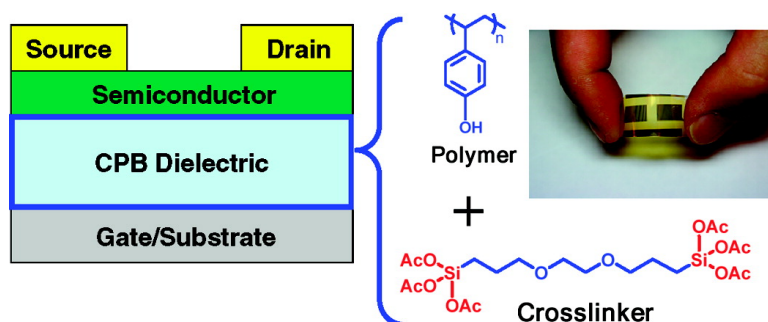


## Printable Cross-Linked Polymer Blend Dielectrics. Design Strategies, Synthesis, Microstructures, and Electrical Properties, with Organic Field-Effect Transistors as Testbeds

Choongik Kim, Zhiming Wang, Hyuk-Jin Choi, Young-Geun Ha, Antonio Facchetti, and Tobin J. Marks

*J. Am. Chem. Soc.*, **2008**, 130 (21), 6867-6878 • DOI: 10.1021/ja801047g • Publication Date (Web): 03 May 2008

Downloaded from <http://pubs.acs.org> on February 8, 2009



### More About This Article

Additional resources and features associated with this article are available within the HTML version:

- Supporting Information
- Access to high resolution figures
- Links to articles and content related to this article
- Copyright permission to reproduce figures and/or text from this article

[View the Full Text HTML](#)

## Printable Cross-Linked Polymer Blend Dielectrics. Design Strategies, Synthesis, Microstructures, and Electrical Properties, with Organic Field-Effect Transistors as Testbeds

Choongik Kim, Zhiming Wang, Hyuk-Jin Choi, Young-Geun Ha, Antonio Facchetti,\* and Tobin J. Marks\*

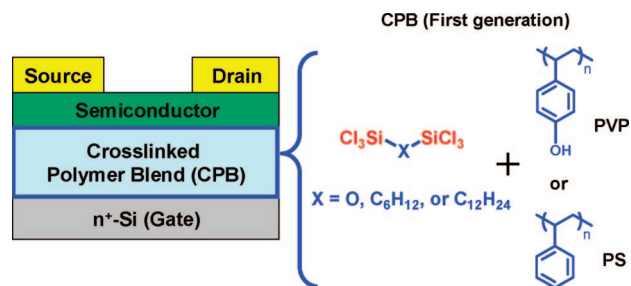
Department of Chemistry and the Materials Research Center, Northwestern University, 2145 Sheridan Road, Evanston, Illinois 60208

Received February 14, 2008; E-mail: a-facchetti@northwestern.edu; t-marks@northwestern.edu

**Abstract:** We report here the synthesis and dielectric properties of optimized, cross-linked polymer blend (CPB) dielectrics for application in organic field-effect transistors (OFETs). Novel silane cross-linking reagents enable the synthesis of CPB films having excellent quality and tunable thickness (from 10 to ~500 nm), fabricated both by spin-coating and gravure-printing. Silane reagents of the formula  $X_3Si-R-SiX_3$  ( $R = -C_6H_{12}-$  and  $X = Cl, OAc, NMe_2, OMe$ , or  $R = -C_2H_4-O-C_2H_4-$  and  $X = OAc$ ) exhibit tunable reactivity with hydroxyl-containing substrates. Dielectric films fabricated by blending  $X_3Si-R-SiX_3$  with poly(4-vinyl)phenol (PVP) require very low-curing temperatures (~110 °C) and adhere tenaciously to a variety of FET gate contact materials such as  $n^+-Si$ , ITO, and Al. The CPB dielectrics exhibit excellent insulating properties (leakage current densities of  $10^{-7} \sim 10^{-8} \text{ A cm}^{-2}$  at 2.0 MV/cm) and tunable capacitance values (from 5 to ~350 nF  $\text{cm}^{-2}$ ). CPB film quality is correlated with the PVP-cross-linking reagent reactivity. OFETs are fabricated with both p- and n-type organic semiconductors using the CPB dielectrics function at low operating voltages. The morphology and microstructure of representative semiconductor films grown on the CPB dielectrics is also investigated and is correlated with OFET device performance.

### Introduction

The development of polymeric gate dielectric materials has been fundamental to the progress of organic electronic circuitry.<sup>1,2</sup> Thus, emerging display and labeling technologies based on organic field-effect transistors (OFETs), such as electronic paper/posters and radiofrequency ID tags, require FET fabrication on flexible plastic substrates over very large areas and via economical, high throughput processes.<sup>3,4</sup> Such technologies will gain wide acceptance only if electronic devices can be produced at significantly lower cost than the current, capital-intensive



**Figure 1.** Schematic of the top-contact/bottom-gate OFET device geometry employed in this study, and the structures of the polymers and silane cross-linkers used for the fabrication of first-generation CPB gate dielectrics.<sup>12</sup>

manufacturing technologies allow. Therefore, there have been worldwide science-based efforts to create, understand, and optimize FET component materials (semiconductor, dielectric, and contacts—Figure 1) which can be deposited via solution-process methodologies such as spin-coating, casting, and printing.<sup>5,6</sup> Regarding organic semiconductors, many are readily deposited from solution either directly or as soluble molecular/polymeric precursors, which are then converted into the insoluble semiconducting form.<sup>7</sup> Regarding conductors, doped conjugated polymers and nanoparticle-based conductive inks allow solution fabrication of sufficiently low resistivity features for source/drain and gate contact patterning.<sup>8</sup> As far as gate dielectrics are concerned, polymers are ideal candidates, and

- (1) (a) Klauk, H. *Organic Electronics: Materials, Manufacturing, and Applications*; Wiley-VCH: Weinheim, Germany, 2006. (b) Deman, A. L.; Tardy, J. *Mater. Sci. Eng., C* **2006**, *26*, 421–426. (c) Klauk, H.; Halik, M.; Zschieschang, U.; Schmid, G.; Radlik, W.; Weber, W. *J. Appl. Phys.* **2002**, *92*, 5259–5263. (d) Sirringhaus, H.; Kawase, T.; Friend, R. H.; Shimoda, T.; Inbasekaran, M.; Wu, W.; Woo, E. P. *Science* **2000**, *290*, 2123–2126.
- (2) Veres, J.; Ogier, S.; Lloyd, G. *Chem. Mater.* **2004**, *16*, 4543–4555.
- (3) (a) Jones, B. A.; Facchetti, A.; Marks, T. J.; Wasielewski, M. R. *Chem. Mater.* **2007**, *19*, 2703–2705. (b) Ji, T.; Kathiresan, M.; Nair, S.; Jung, S.; Natarajan, V.; Vishnubhatia, R. M. R.; Varadan, V. K. *Proc. SPIE-Int. Soc. Opt. Eng.* **2007**, *6528*, 1–6. (c) Yoo, B.; Jung, T. O.; Basu, D.; Dodabalapur, A.; Jones, B. A.; Facchetti, A.; Wasielewski, M. R.; Marks, T. J. *Appl. Phys. Lett.* **2006**, *88*, 082104/1–3. (d) Subramanian, V.; Chang, P. C.; Lee, J. B.; Molesa, S. E.; Volkman, S. K. *IEEE Trans. Compon. Packag. Technol.* **2005**, *28*, 742–747. (e) Baude, P. F.; Ender, D. A.; Haase, M. A.; Kelley, T. W.; Muryes, D. V.; Theiss, S. D. *Appl. Phys. Lett.* **2003**, *82*, 3964–3966. (f) Drury, C. J.; Mutsaers, C. M. J.; Hart, C. M.; Matters, M.; de Leeuw, D. M. *Appl. Phys. Lett.* **1998**, *73*, 108–110. (g) Gamota, D. R.; Brazis, P.; Kalyanasundaram, X.; Zhang, J. *Printed Organic and Molecular Electronics*; Kluwer Academic Publishers: New York, 2004.

- (4) Singh, T. B.; Sariciftci, N. S. *Annu. Rev. Mater. Res.* **2006**, *36*, 199–230.

most of the polymer dielectrics employed to date for OFETs are commercially available, exhibiting a large range of dielectric constants and acceptable solubility in a variety of solvents.<sup>9,10</sup>

A typical OFET structure is shown in Figure 1. In this device, the conductance of the source-drain channel region is modulated by the source-gate electric field ( $E_G$ ). When the device is in the off-state ( $E_G = 0$ ) the channel conductance is very low (typically  $< 10^{-12}$  S), whereas in the on-state ( $E_G \neq 0$ ) a sharp increase in conductance is observed ( $> 10^{-6}$  S), with output currents (in saturation) defined as in<sup>11</sup>

$$I_{DS} = \frac{W}{2L} \mu C_i (V_G - V_T)^2 \quad (1)$$

where  $WL$  is the channel width/length,  $C_i$  is the dielectric capacitance per unit area,  $V_G$  is the source-gate voltage, and  $V_T$  is the threshold voltage. Among the key device parameters are the semiconductor field-effect mobility ( $\mu$ ) and the device

current on/off ratio ( $I_{on}/I_{off}$ ). The gate insulator affects device performance in many ways, principally permitting the creation of the gate field and establishing a two-dimensional channel charge sheet. The accumulated charge carriers transit from the source to the drain electrodes in an area very close to the dielectric-semiconductor interface upon application of a source-drain bias. Therefore, the nature of the semiconductor-dielectric interface, hence the dielectric surface morphology prior to semiconductor deposition, greatly affects how the accumulated charges move in the semiconductor and, therefore, the field-effect mobility.<sup>13</sup> Furthermore, the dielectric morphology and surface energy tuning (e.g., surface treatment via a self-assembled monolayer) have been shown to significantly modify the growth, morphology, and microstructure of the overlying vapor/solution-deposited semiconductor—factors all affecting  $\mu$  and  $I_{on}/I_{off}$ .<sup>14</sup> The gate insulator dielectric properties also affect the proximate semiconductor density of states distribution for both amorphous and single-crystal semiconductors.<sup>15</sup> Also critical for long-term device stability is the extent to which the dielectric surface traps charge carriers via reactive chemical groups, and the density of interfacial states and charged species.<sup>16</sup>

There are three major limitations to current-generation polymer gate dielectric-based OFETs. The first is that, with few exceptions,<sup>12,17</sup> they function at relatively large operating voltages, reflecting the intrinsically low (compared to crystalline

- (5) (a) Herlogsson, L.; Crispin, X.; Robinson, N. D.; Sandberg, M.; Hagel, O.-J.; Gustafsson, G.; Berggren, M. *Adv. Mater.* **2007**, *19*, 97–101. (b) Yildirim, F. A.; Ucurum, C.; Schlieue, R. R.; Bauhofer, W.; Meixner, R. M.; Goebel, H.; Krautschnieder, W. *Appl. Phys. Lett.* **2007**, *90*, 083501/1–3. (c) Itoh, E.; Miyairi, K. *Thin Solid Films* **2006**, *499*, 95–103. (d) Kim, Y. M.; Lim, E.; Kang, I.-N.; Jung, B.-J.; Lee, J.; Koo, B. W.; Do, L.-M.; Shim, H.-K. *Macromolecules* **2006**, *39*, 4081–4085. (e) Yang, S. Y.; Shin, K.; Park, C. E. *Adv. Funct. Mater.* **2005**, *15*, 1806–1814. (f) Naber, R. C. G.; Tanase, C.; Blom, P. W. M.; Gelinck, G. H.; Marsman, A. W.; Touwslager, F. J.; Setayesh, S.; de Leeuw, D. M. *Nat. Mater.* **2005**, *4*, 243–248. (g) Liu, Y.; Varshramyan, K.; Cui, T. *Macromol. Rapid Commun.* **2005**, *26*, 1955–1959. (h) Granstrom, J.; Katz, H. E. *J. Mater. Res.* **2004**, *19*, 3540–3546. (i) Shtein, M.; Peumans, P.; Benziger, J. B.; Forrest, S. R. *Adv. Mater.* **2004**, *16*, 1615–1620. (j) Knobloch, A.; Manuelli, A.; Bernds, A.; Clemens, W. *J. Appl. Phys.* **2004**, *96*, 2286–2291.
- (6) Bao, Z.; Rogers, J. A.; Katz, H. E. *J. Mater. Chem.* **1999**, *9*, 1895–1904.
- (7) (a) Facchetti, A. *Mater. Today* **2007**, *10*, 28–37. (b) Payne, M. M.; Parkin, S. R.; Anthony, J. E.; Kuo, C.-C.; Jackson, T. N. *J. Am. Chem. Soc.* **2005**, *127*, 4986–4987. (c) Afzali, A.; Kagan, C. R.; Traub, G. P. *Synth. Met.* **2005**, *155*, 490–494. (d) Afzali, A.; Dimitrakopoulos, C. D.; Breen, T. L. *J. Am. Chem. Soc.* **2002**, *124*, 8812–8813. (e) Herwig, P. T.; Müllen, K. *Adv. Mater.* **1999**, *11*, 480–483. (f) Brown, A. R.; Pomp, A.; de Leeuw, D. M.; Klaassen, D. B. M.; Havinga, E. E.; Herwig, P.; Müllen, K. *J. Appl. Phys.* **1996**, *79*, 2136–2138.
- (8) (a) Gamberth, S.; Klug, A.; Scheibrer, H.; Scherf, U.; Moderegger, E.; List, E. J. W. *Adv. Funct. Mater.* **2007**, *17*, 3111–3118. (b) Kim, D.; Jeong, S.; Moon, J.; Han, S.; Chung, J. *Appl. Phys. Lett.* **2007**, *91*, 071114/1–3. (c) Ko, S. H.; Pan, H.; Grigoropoulos, C. P.; Luscombe, C. K.; Frechet, J. M. J.; Poulidakos, D. *Appl. Phys. Lett.* **2007**, *90*, 141103/1–3. (d) Noguchi, Y.; Sekitani, T.; Someya, T. *Appl. Phys. Lett.* **2006**, *89*, 253507/1–3. (e) Stutzmann, N.; Friend, R. H.; Sirringhaus, H. *Science* **2003**, *299*, 1881–1884. (f) Pron, A.; Rannou, P. *Prog. Polym. Sci.* **2002**, *27*, 135–190.
- (9) Facchetti, A.; Yoon, M.-H.; Marks, T. J. *Adv. Mater.* **2005**, *17*, 1705–1725.
- (10) (a) Kaake, L. G.; Zou, Y.; Panzer, M. J.; Frisbie, C. D.; Zhu, X.-Y. *J. Am. Chem. Soc.* **2007**, *129*, 7824–7830. (b) Noh, S. H.; Choi, W.; Oh, M. S.; Hwang, D. K.; Lee, K.; Im, S.; Jang, S.; Kim, E. *Appl. Phys. Lett.* **2007**, *90*, 253504/1–3. (c) Bae, J.-H.; Kim, J.; Kim, W.-H.; Lee, S.-D. *Jpn. J. Appl. Phys.* **2007**, *46*, 385–389. (d) Zhao, Y.; Dong, G.; Wang, L.; Qiu, Y. *Appl. Phys. Lett.* **2007**, *90*, 252110/1–3. (e) Ghim, J.; Baeg, K.-J.; Noh, Y.-Y.; Kang, S.-J.; Jo, J.; Kim, D.-Y.; Cho, S.; Yuen, J.; Lee, K.; Heeger, A. J. *Appl. Phys. Lett.* **2006**, *89*, 202516/1–3. (f) Lee, K.; Kim, J. H.; Im, S. *Appl. Phys. Lett.* **2006**, *88*, 023504/1–3. (g) Unni, K. N. N.; Dabos-Seignon, S.; Nunzi, J.-M. *J. Mater. Sci.* **2006**, *41*, 317–322. (h) Sung, J. H.; Park, S. J.; Park, J. H.; Choi, H. J.; Choi, J. S. *Synth. Met.* **2006**, *156*, 861–864. (i) Lee, J.; Hwang, D. K.; Choi, J.-M.; Lee, K.; Kim, J. H.; Im, S.; Park, J. H.; Kim, E. *Appl. Phys. Lett.* **2005**, *87*, 023504/1–3. (j) Park, S. Y.; Park, M.; Lee, H. H. *Appl. Phys. Lett.* **2004**, *85*, 2283–2285. (k) Gelinck, G. H.; Geuns, T. C. T.; de Leeuw, D. M. *Appl. Phys. Lett.* **2000**, *77*, 1487–1489.
- (11) Sze, S. M. *Semiconductor Devices: Physics and Technology*; 2nd ed.; Wiley: New York, 1981.
- (12) Yoon, M.-H.; Yan, H.; Facchetti, A.; Marks, T. J. *J. Am. Chem. Soc.* **2005**, *127*, 10388–10395.
- (13) (a) Park, Y. D.; Lim, J. A.; Lee, H. S.; Cho, K. *Mater. Today* **2007**, *10*, 46–54. (b) Surin, M.; Leclere, Ph.; Lazzaroni, R.; Yuen, J. D.; Wang, G.; Moses, D.; Heeger, A. J.; Cho, S.; Lee, K. *J. Appl. Phys.* **2006**, *100*, 033712/1–6. (c) Lee, C. A.; Park, D. W.; Jin, S. H.; Park, I. H.; Lee, J. D.; Park, B.-G. *Appl. Phys. Lett.* **2006**, *88*, 252102/1–3. (d) Chua, L.-L.; Zausmell, J.; Chang, J.-F.; Ou, E. C.-W.; Ho, P. K.-H.; Sirringhaus, H.; Friend, R. H. *Nature* **2005**, *434*, 194–199. (e) Panzer, M. J.; Frisbie, C. D. *J. Am. Chem. Soc.* **2005**, *127*, 6960–6961. (f) Schroeder, R.; Majewski, L. A.; Grell, M. *Adv. Mater.* **2005**, *17*, 1535–1539. (g) Kobayashi, S.; Nishikawa, T.; Takenobu, T.; Mori, S.; Shimoda, T.; Mitani, T.; Shimotani, H.; Yoshimono, N.; Ogawa, S.; Iwasa, Y. *Nat. Mater.* **2004**, *3*, 317–322. (h) Pernstich, K. P.; Haas, S.; Oberhoff, D.; Goldmann, C.; Gundlach, D. J.; Batlogg, B.; Rashid, A. N.; Schitter, G. *J. Appl. Phys.* **2004**, *96*, 6431–6438. (i) Dimitrakopoulos, C. D.; Purushothaman, S.; Kymissis, J.; Callegari, A.; Shaw, J. M. *Science* **1999**, *283*, 822–824.
- (14) (a) Yoon, M.-H.; Kim, C.; Facchetti, A.; Marks, T. J. *J. Am. Chem. Soc.* **2006**, *128*, 12851–12869. (b) Hamadani, B. H.; Corley, D. A.; Cizek, J. W.; Tour, J. M.; Natelson, D. *Nano Lett.* **2006**, *6*, 1303–1306. (c) Lee, H. S.; Kim, D. H.; Cho, J. H.; Park, Y. D.; Kim, J. S.; Cho, K. *Adv. Funct. Mater.* **2006**, *16*, 1859–1864. (d) Tsukagoshi, K.; Shiget, K.; Yagi, I.; Aoyagi, Y. *Appl. Phys. Lett.* **2006**, *89*, 113507/1–3. (e) DeLongchamp, D. M.; Sambasivan, S.; Fischer, D. A.; Lin, E. K.; Chang, P.; Murphy, A. R.; Frechet, J. M. J.; Subramanian, V. *Adv. Mater.* **2005**, *17*, 2340–2344. (f) Salleo, A.; Chabinc, M. L.; Yang, M. S.; Street, R. A. *Appl. Phys. Lett.* **2002**, *81*, 4383–4385. (g) Lin, Y. Y.; Gundlach, D. J.; Nelson, S. F.; Jackson, T. N. *IEEE Electron Device Lett.* **1997**, *18*, 606–608.
- (15) (a) Wang, A.; Kymissis, I.; Bulovic, V.; Ibitayo, A. *IEEE Trans. Electron Devices* **2006**, *53*, 9–13. (b) Lang, D. V.; Chi, X.; Siegrist, T.; Sergent, A. M.; Ramirez, A. P. *Phys. Rev. Lett.* **2004**, *93*, 086802/1–4.
- (16) (a) Goldmann, C.; Krellner, C.; Pernstich, K. P.; Haas, S.; Gundlach, D. J.; Batlogg, B. *J. Appl. Phys.* **2006**, *99*, 034507/1–8. (b) Gomes, H. L.; Stallinga, P.; Colle, M.; Biscarini, F.; de Leeuw, D. M. *J. Non-Cryst. Solids* **2006**, *352*, 1761–1764. (c) Gu, G.; Kane, M. G.; Doty, J. E.; Firester, A. H. *Appl. Phys. Lett.* **2005**, *87*, 243512/1–3.
- (17) (a) Hwang, D. K.; Lee, K.; Kim, J. H.; Im, S.; Kim, C. S.; Baik, H. K.; Park, J. H.; Kim, E. *Appl. Phys. Lett.* **2006**, *88*, 243513/1–3. (b) Yang, S. Y.; Kim, S. H.; Shin, K.; Jeon, H.; Park, C. E. *Appl. Phys. Lett.* **2006**, *88*, 173507/1–3. (c) Jang, Y.; Kim, D. H.; Park, Y. D.; Cho, J. H.; Hwang, M.; Cho, K. *Appl. Phys. Lett.* **2006**, *88*, 072101/1–3. (d) Panzer, M. J.; Newman, C. R.; Frisbie, C. D. *Appl. Phys. Lett.* **2005**, *86*, 103503/1–3.



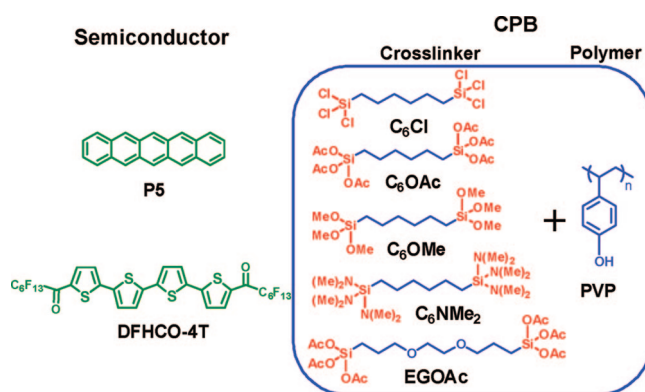
inorganic semiconductors) field-effect mobilities.<sup>18</sup> Second, very few polymeric dielectrics perform optimally with a broad variety of both hole- and electron-transporting organic semiconductors, limiting organic complementary circuit applications. Third, it is very difficult with the same polymer formulation to realize nanoscopically thin films exhibiting large capacitance values but having minimal gate leakage current at useful gate fields. From eq 1, an attractive means to address the first problem, while maintaining all the other parameters constant, would be to substantially increase the gate  $C_i$ , which would allow achieving the same current but at significantly lower  $V_G$  values. Since

$$C_i = \epsilon_0 \frac{k}{d} \quad (2)$$

where  $k$  is the dielectric constant,  $\epsilon_0$  is the vacuum permittivity, and  $d$  is the insulator thickness.  $C_i$  is increased as  $k$  increases and/or  $d$  decreases. However, the  $k$  value of most insulating polymers is confined within a relatively narrow range (ca. 2–6) and, equally important, the films must be very thick (usually  $\sim 1 \mu\text{m}$ ) to avoid significant leakage currents to the gate electrode.<sup>9,19</sup> To reduce leakage currents for thinner films, cross-linked polymer dielectrics such as melamine–poly(4-vinyl)phenol (PVP) and cross-linked BCB (benzocyclobutene) have been introduced,<sup>20</sup> which allow reducing the dielectric thickness. However, films of these materials require high annealing temperatures ( $> 150$ – $200 \text{ }^\circ\text{C}$ ) and  $C_i$  values are typically  $< 20 \text{ nF cm}^{-2}$ .

Recently, we demonstrated that blending appropriate  $\pi$ -electron polymers, for example, PVP and PS, with chlorosilane cross-linking reagents affords robust, adherent, pinhole-free, high-capacitance, low-leakage, ultrathin (10–20 nm) gate dielectric materials (Figure 1).<sup>12</sup> However, owing to the high reactivity of the chlorosilane cross-linking reagents and unoptimized cross-linking reactions, the resulting dielectric materials prepared by spin-coating and post-annealing exhibit less than optimum surface morphologies (rms roughness  $> 2 \text{ nm}$ ), compromising OFET performance, especially the field-effect charge carrier mobility. Furthermore, to enable deposition of the CPB films via roll-to-roll processes, hence by printing methodologies, it is of fundamental importance to control the kinetics of cross-linking to avoid premature cross-linked matrix formation in solution before film deposition. Note that with current printing technologies, relatively thick (a few  $\mu\text{ms}$ ) dielectric films can be deposited for many applications.<sup>3g</sup>

In this contribution, we report on the design, synthesis, and implementation of new silane cross-linkers having tuned



**Figure 2.** Structures of the organic semiconductor (left) and of the CPB precursors (polymer and silane cross-linkers, right) employed in this study.

reactivity with respect to hydroxyl-containing dielectric polymers (Figure 2). For the first time, an in situ kinetic study comparing the reactivity of chloro-, acetoxy-, dialkylamino-, and methoxy-silanes with a hydroxylated reactant is reported. This study thereby affords a correlation of cross-linker-polymer reactivity patterns with the corresponding CPB dielectric properties. With the new silane cross-linkers, we demonstrate that optimization of cross-linking conditions, especially by using moderately reactive cross-linking reagents, appropriate solvents, and polymer/cross-linker molar ratio, affords very low leakage and *very smooth* dielectric films. These new CPB formulations enable tunable thickness and capacitances and can be fabricated on conventional Si substrates as well as on flexible Al/PEN and ITO/Mylar substrates via spin-coating and gravure printing. OFETs fabricated with these new CPB dielectric films exhibit good performance for both p-(pentacene) and n-type (DFHCO-4T<sup>21</sup>) organic semiconductors (Figure 2). Finally, the hydrophilic properties of the polymer and siloxane matrices in the CPB films are correlated with humidity-dependent dielectric properties and the resulting OFET device response.

## Results

**Strategy for Cross-Linking Reagent Design.** The CPB materials reported here consist of poly(4-vinyl)phenol (PVP) chains covalently bound in cross-linked matrices (Figure 2). As in the case of other cross-linked polymers employed for diverse applications,<sup>12,20</sup> this methodology enhances structural robustness and, for organic electronic applications, electrical insulating properties. The present cross-linking strategy employs the coupling reaction of selected bifunctional organosilane reagents with OH-functionalized molecules/polymers and/or with  $\text{H}_2\text{O}$  to produce robust siloxane networks (Scheme 1). We previously reported that when chlorosilanes are used in combination with PVP (or polystyrene), cross-linked matrices are produced in air immediately after film deposition and curing. Moreover, the film structural integrity and connectivity of these materials are evident by the complete insolubility of the product in the mother solution (Figure 2).<sup>12</sup> The curing temperature ( $\sim 110 \text{ }^\circ\text{C}$ ) is fully compatible with the common varieties of plastic substrates employed in organic electronics.<sup>1a,3g</sup>

Previous CPB dielectrics based on chlorosilane cross-linkers afford relatively rough dielectric film surfaces (rms roughness  $> 2 \text{ nm}$  for 10–20 nm thick films) due to the great reactivity of

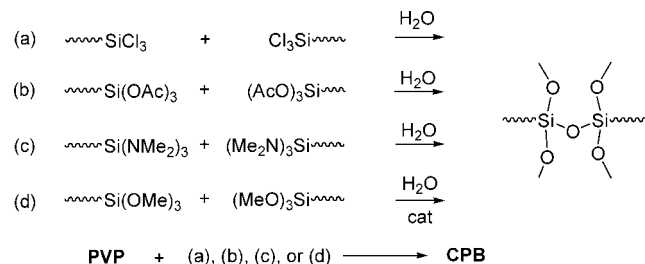
(18) Dimitrakopoulos, C. D.; Malenfant, P. R. L. *Adv. Mater.* **2002**, *14*, 99–117.

(19) (a) Singh, T. B.; Meghdadi, F.; Günes, S.; Marjanovic, N.; Horowitz, G.; Lang, P.; Bauer, S.; Sariciftci, N. S. *Adv. Mater.* **2005**, *17*, 2315–2320. (b) Nunes, G., Jr.; Zane, S. G.; Meth, J. S. *J. Appl. Phys.* **2005**, *98*, 104503/1–6.

(20) (a) Lim, S. C.; Kim, S. H.; Koo, J. B.; Lee, J. H.; Ku, C. H.; Yang, Y. S.; Zyung, T. *Appl. Phys. Lett.* **2007**, *90*, 173512/1–3. (b) Lee, S. H.; Choo, D. J.; Han, S. H.; Kim, J. H.; Son, Y. R.; Jang, J. *Appl. Phys. Lett.* **2007**, *90*, 033502/1–3. (c) Kim, S. H.; Yang, S. Y.; Shin, K.; Jeon, H.; Lee, J. W.; Hong, K. P.; Park, C. E. *Appl. Phys. Lett.* **2006**, *89*, 183516/1–3. (d) Marjanovic, N.; Singh, T. B.; Dennler, G.; Günes, S.; Neugebauer, H.; Sariciftci, N. S.; Schwödiauer, R.; Bauer, S. *Org. Electron.* **2006**, *7*, 188–194. (e) Jang, Y.; Kim, D. H.; Park, Y. D.; Cho, J. H.; Hwang, M.; Cho, K. *Appl. Phys. Lett.* **2005**, *87*, 152105/1–3. (f) Singh, T. B.; Marjanovic, N.; Stadler, P.; Auinger, M.; Matt, G. J.; Günes, S.; Sariciftci, N. S.; Schwödiauer, R.; Bauer, S. *J. Appl. Phys.* **2005**, *97*, 083714/1–5. (g) Chua, L.-L.; Ho, P. K. H.; Sirringhaus, H.; Friend, R. H. *Appl. Phys. Lett.* **2004**, *84*, 3400–3402.

(21) Yoon, M.-H.; DiBenedetto, S. A.; Facchetti, A.; Marks, T. J. *J. Am. Chem. Soc.* **2005**, *127*, 1348–1349.

**Scheme 1.** Schematic of the Crosslinking Processes for the Various Organosilane Crosslinking Reagents Employed in This Study

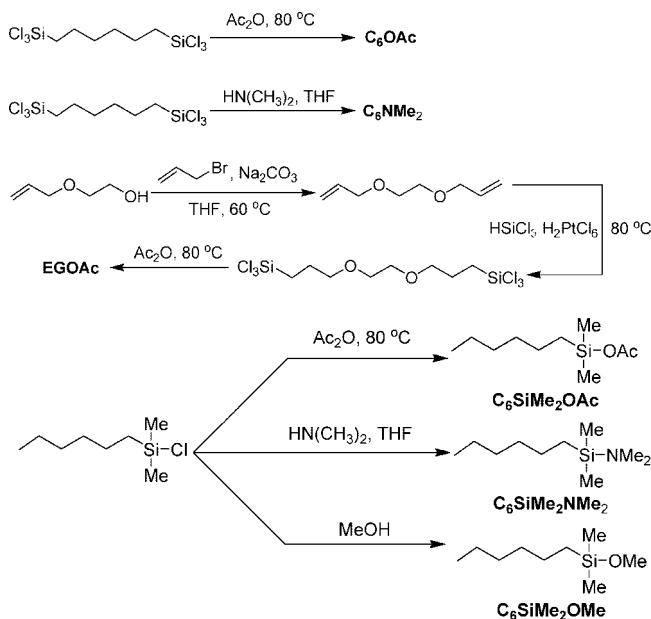


the cross-linking reagents.<sup>12</sup> Furthermore, for the same reason, chlorosilane-based dielectric formulations cannot be readily printed (*vide infra*). To optimize cross-linking reaction conditions, leading to robust, printable films and smoother dielectric surface morphologies, as well as to assess the influence of different CPB cross-linking formulations, the combination of PVP with a variety of  $\alpha$ - $\omega$ -hexyl cross-linking reagents, differing in the cross-linkable silane end groups and core structures, was explored, including 1,6-bis(trichlorosilyl)hexane ( $\text{C}_6\text{Cl}$ ; as a reference), 1,6-bis(triacetoxysilyl)hexane ( $\text{C}_6\text{OAc}$ ), 1,6-bis[tri(dimethylamino)silyl]hexane ( $\text{C}_6\text{NMe}_2$ ), and 1,6-bis(trimethoxysilyl)hexane ( $\text{C}_6\text{OMe}$ ; Figure 2). The  $\alpha$ , $\omega$ -hexyl ( $\text{C}_6$ ) linker was chosen because it was previously found to afford the smoothest film surface morphology when used as a chlorosilane-based cross-linker.<sup>12</sup> The dioxyethylene-containing core in the EGOAc cross-linker was selected because of the improved chemical compatibility with PVP, leading to more complete cross-linking and smoother dielectric surfaces (*vide infra*).

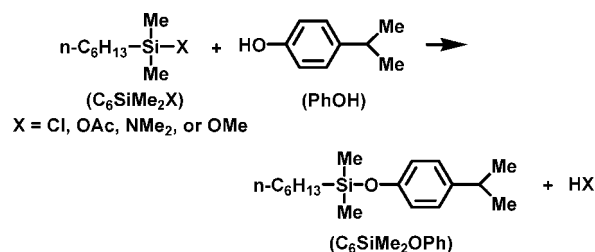
**Cross-Linker Synthesis.** The reagents 1,6-bis(triacetoxysilyl)hexane ( $\text{C}_6\text{OAc}$ ), bis(3-triacetoxysilylpropyl ethylene ether) (EGOAc), 1,6-bis(tri(dimethylamino)silyl)hexane ( $\text{C}_6\text{NMe}_2$ ), dimethylhexylacetoxysilane ( $\text{C}_6\text{SiMe}_2\text{OAc}$ ), dimethylhexyl(dimethylamino)silane ( $\text{C}_6\text{SiMe}_2\text{NMe}_2$ ) and dimethylhexylmethoxysilane ( $\text{C}_6\text{SiMe}_2\text{OMe}$ ) were synthesized as shown in Scheme 2.  $\text{C}_6\text{OAc}$  and  $\text{C}_6\text{NMe}_2$  were obtained in almost quantitative yields by reaction of 1,6-bis(trichlorosilyl)hexane with acetic anhydride and dimethylamine, respectively. Similarly,  $\text{C}_6\text{SiMe}_2\text{OAc}$ ,  $\text{C}_6\text{SiMe}_2\text{NMe}_2$ , and  $\text{C}_6\text{SiMe}_2\text{OMe}$  (model reagents employed for the kinetic study, *vide infra*) were synthesized by reaction of commercially available dimethylhexylchlorosilane ( $\text{C}_6\text{SiMe}_2\text{Cl}$ ) with acetic anhydride, dimethylamine, or anhydrous methanol, respectively. EGOAc was synthesized in three steps: (1) allylation of 2-allyloxy-ethanol in the presence of allyl bromide and sodium hydride (or anhydrous sodium carbonate) to form diallylethylene ether; (2) hydrosilylation of diallylethylene ether with trichlorosilane to afford [bis(3-trichlorosilyl)propyl] ethylene ether; (3) functional group conversion of [bis(3-trichlorosilyl)propyl] ethylene ether with acetic anhydride to yield EGOAc in 60% overall yield. The chemical structures and purities of the new silane cross-linking reagents were verified by  $^1\text{H}$  and  $^{29}\text{Si}$  NMR as well as by elemental analysis.

**Kinetic Study.** The kinetics of nucleophilic substitution reactions of organosilicon compounds have been reported in previous literature. In most studies, halosilanes and water (or alcohols) were chosen as substrates and nucleophiles, respectively. In absence of catalysts, a pseudo-first-order chlorosilane hydrolysis (alcoholysis) reaction was studied using conventional techniques such as sampling and titration. Second-order rate coefficients ( $k \approx 10^{-4} \text{ L mol}^{-1} \text{ s}^{-1}$  for chlorotriisopropylsilane in dioxane) were determined and an  $\text{S}_{\text{N}}2$ -type mechanism

**Scheme 2.** Synthesis of the New CPB Crosslinking Reagents ( $\text{C}_6\text{OAc}$ ,  $\text{C}_6\text{NMe}_2$ , EGOAc) and Model Substrates Used for the Kinetic Study ( $\text{C}_6\text{SiOAc}$ ,  $\text{C}_6\text{SiNMe}_2$ , and  $\text{C}_6\text{SiOMe}$ )



**Scheme 3.** Model Reactions of Functional Silanes ( $\text{C}_6\text{SiMe}_2\text{Cl}$ ,  $\text{C}_6\text{SiMe}_2\text{OAc}$ ,  $\text{C}_6\text{SiMe}_2\text{NMe}_2$ , and  $\text{C}_6\text{SiMe}_2\text{OMe}$ ) with 4-Isopropylphenol (PhOH)



proposed. The presence of catalysts may lead to more complex reaction kinetics and mechanisms, which depend on the nucleophilicity of the catalyst and the reaction stereochemistry.<sup>22</sup>

The surface morphologies of the cross-linked dielectric films depend strongly on the PVP coupling rate with the chosen silane cross-linker. Therefore, the reactivities of the silane cross-linker leaving groups (chloro-, acetoxy-, dimethylamino-, and methoxy) were quantified using model reactions. To simplify the kinetic study of the coupling reactions, monofunctional silanes, including dimethylhexylchlorosilane ( $\text{C}_6\text{SiMe}_2\text{Cl}$ ), dimethylhexylacetoxysilane ( $\text{C}_6\text{SiMe}_2\text{OAc}$ ), dimethylhexyl(dimethylamino)silane ( $\text{C}_6\text{SiMe}_2\text{NMe}_2$ ), and dimethylhexylmethoxysilane ( $\text{C}_6\text{SiMe}_2\text{OMe}$ ) were used to model the cross-linker reagents, and 4-isopropylphenol (PhOH) was chosen as a substrate to model PVP (Scheme 3). In contrast to the kinetic studies at room temperature in the presence of condensation catalysts reported by others,<sup>22</sup> reactions here were carried out at 110 °C without added catalyst, similar to the conditions employed for the polymer-cross-linker reactions leading to the CPB dielectric films.

The product of the reaction is dimethylhexyl-4-isopropylphenoxysilane ( $\text{C}_6\text{SiMe}_2\text{OPh}$ ), independent of the silane reagent.

(22) (a) Sommer, L. H. *Stereochemistry, Mechanism and Silicon*; McGraw-Hill, Inc.: New York, 1965. (b) Rubinsztajn, S.; Cypryk, M.; Chojnowski, J. *J. Organomet. Chem.* **1989**, *367*, 27–37. (c) Corriu, R. J. P.; Dabosi, G.; Martineau, M. *J. Chem. Soc., Chem. Commun.* **1977**, 649–650.

**Table 1.**  $^1\text{H}$  NMR and Kinetic Data for Model Reactions of Functional Silanes with 4-Isopropylphenol (PhOH)

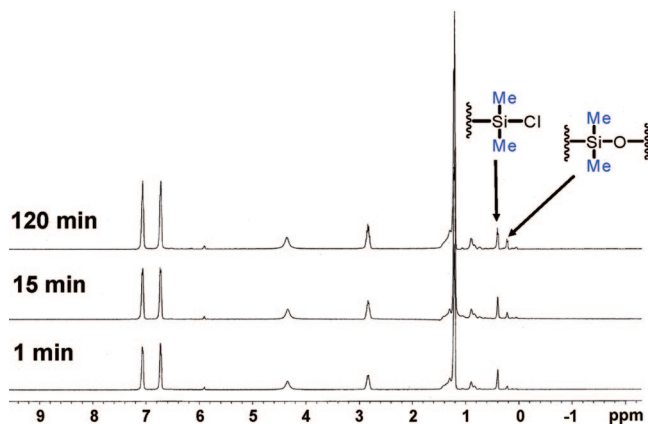
Compound	$^1\text{H}$ NMR ( $\text{CDCl}_3$ )	$k$ ( $\text{L mol}^{-1} \text{s}^{-1}$ )
$\text{C}_6\text{SiMe}_2\text{NMe}_2$	$\text{CH}_3\text{CH}_2\text{CH}_2\text{CH}_2\text{CH}_2\text{CH}_2\text{Si}(\text{CH}_3)_2(\text{N}(\text{CH}_3)_2)$ 2.42 (s, 6H), 1.32 (m, 8H), 0.88 (t, 3H), 0.58 (t, 2H), 0.08 (s, 6H)	too fast to measure
$\text{C}_6\text{SiMe}_2\text{Cl}$	$\text{CH}_3\text{CH}_2\text{CH}_2\text{CH}_2\text{CH}_2\text{CH}_2\text{Si}(\text{CH}_3)_2\text{Cl}$ 1.42–1.15 (m, 8H), 0.85 (t, 3H), 0.78 (t, 2H), 0.38 (s, 6H)	$8.78 \times 10^{-5}$
$\text{C}_6\text{SiMe}_2\text{OAc}$	$\text{CH}_3\text{CH}_2\text{CH}_2\text{CH}_2\text{CH}_2\text{CH}_2\text{Si}(\text{CH}_3)_2(\text{OCOCH}_3)$ 2.03 (s, 3H), 1.45–1.18 (m, 8H), 0.86 (t, 3H), 0.72 (t, 2H), 0.22 (s, 6H)	$4.37 \times 10^{-6}$
$\text{C}_6\text{SiMe}_2\text{OMe}$	$\text{CH}_3\text{CH}_2\text{CH}_2\text{CH}_2\text{CH}_2\text{CH}_2\text{Si}(\text{CH}_3)_2(\text{OCH}_3)$ 3.55 (s, 3H), 1.32 (m, 8H), 0.90 (t, 3H), 0.52 (t, 2H), 0.05 (s, 6H)	no reaction
$\text{C}_6\text{SiMe}_2\text{OPh}$	$\text{CH}_3\text{CH}_2\text{CH}_2\text{CH}_2\text{CH}_2\text{CH}_2\text{Si}(\text{CH}_3)_2(\text{OPhCH}(\text{CH}_3)_2)$ 7.09 (d, 2H), 6.77 (d, 2H), 2.85 (m, 1H), 1.40–1.18 (m, 14H), 0.86 (t, 3H), 0.72 (t, 2H), 0.23 (s, 6H)	
PhOH	$\text{HOPhCH}(\text{CH}_3)_2$ 7.10 (d, 2H), 6.85 (d, 2H), 4.85 (s, 1H), 2.85 (m, 1H), 1.20 (d, 6H)	

The chemical shift of the Si-CH<sub>3</sub> groups is sensitive to the leaving group (Table 1). For example, as the reaction proceeds, the resonance intensity at  $\delta$  0.38 ppm assigned to the  $\text{C}_6\text{SiMe}_2\text{Cl}$  methyl groups decreases, while the product  $\text{C}_6\text{SiMe}_2\text{OPh}$  methyl signal located at  $\delta$  0.23 ppm increases in intensity (Figure 3). Hence, based on the Si-CH<sub>3</sub> group peak intensities, the concentration of monofunctional silane reagents was monitored over time (2 h) by in situ  $^1\text{H}$  NMR. The model reaction kinetics obey the empirical rate law:  $R_p = k[\text{PhOH}][\text{C}_6\text{SiMe}_2\text{X}]$  over a wide range of concentrations where  $R_p$  is reaction rate and  $k$  is rate constant (Figure 4). As shown in Table 1, the reactivity of the silane functional group decreases in the order  $\text{NMe}_2 \gg \text{Cl} > \text{OAc} \gg \text{OMe}$ . The rate constant for  $\text{C}_6\text{SiMe}_2\text{Cl}$  ( $8.78 \times 10^{-5} \text{ L mol}^{-1} \text{ s}^{-1}$ ) is comparable to (slightly lower than) the alcoholysis rate constant of chlorotriisopropylsilane ( $\sim 1.5 \times 10^{-4} \text{ L mol}^{-1} \text{ s}^{-1}$ ), but less than that of chlorotriisopropylsilane

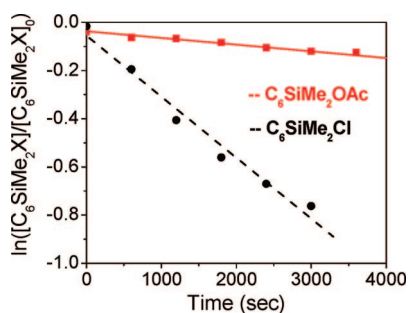
( $\sim 6 \times 10^{-4} \text{ L mol}^{-1} \text{ s}^{-1}$ ). As will be shown later, these data are in excellent accord with the observed CPB surface morphological characteristics, film robustness, and dielectric characteristics of the films fabricated with the various silane cross-linkers (vide infra).

**CPB Film Fabrication and Characterization.** To enable deposition of CPB films via printing, it is important to control and optimize the cross-linking conditions to produce robust films with smooth surface morphologies. Moreover, acceptable OFET response parameters must be achieved using concentrated polymer/cross-linker solutions having appropriate rheologies for printing. In previous studies, the relatively thick CPB films fabricated by gravure printing and spin-coating<sup>12</sup> using highly reactive chlorosilane-based cross-linking reagents (vide infra) did not afford optimal microstructural and dielectric properties. Therefore, spin-coated ultrathin (<20 nm) CPB films were first investigated in the present study to determine how different cross-linking reagent reactivities affect CPB film dielectric properties. Similar optimization was then performed for thicker (50–300 nm) spin-coated CPB films to understand how/if thicker CPB film properties differ from those of the corresponding ultrathin films. Finally, the cross-linking reagents affording optimum dielectric properties for spin-coated thick CPB films were selected for gravure-printing experiments. For comparison purposes, all leakage current density and capacitance measurements are carried out under vacuum and selected samples then are tested in various atmospheres.

**a. Spin-Coated Ultrathin (<20 nm) CPB Films.** When employing a new cross-linker, it is first necessary to reoptimize film deposition conditions by varying parameters such as solvent type and polymer/cross-linker stoichiometric ratio. The goal is to achieve, for a specific film thickness range, optimal film robustness and a smooth dielectric surface. Since a smooth dielectric-semiconductor interface is a prerequisite for efficient charge transport in the FET channel,<sup>23</sup> the visual appearance of the film combined with AFM data provide important information for initial materials screening and evaluation. Table 2 summarizes an example describing the optimization of  $\sim 15$  nm-thick spin-coated CPB films fabricated with PVP- $\text{C}_6\text{OAc}$ , by varying the deposition solvent and polymer/cross-linker ratio. Note that a similar procedure was performed for each cross-linker. Independent of the polymer/cross-linker ratio, EtOAc was found to be the optimum solvent for depositing CPB films prepared from PVP- $\text{C}_6\text{OAc}$ , affording very smooth surfaces (rms



**Figure 3.**  $^1\text{H}$  NMR spectra of a  $\text{C}_6\text{SiMe}_2\text{Cl}$  + PhOH mixture recorded at different reaction times ( $t = 1, 15,$  and  $120$  min, from bottom to top) in  $\text{C}_2\text{D}_2\text{Cl}_4$  at  $110$  °C.



**Figure 4.** Typical kinetic plot of  $\ln([\text{C}_6\text{SiMe}_2\text{X}]/[\text{C}_6\text{SiMe}_2\text{X}]_0)$  versus reaction time with PhOH.

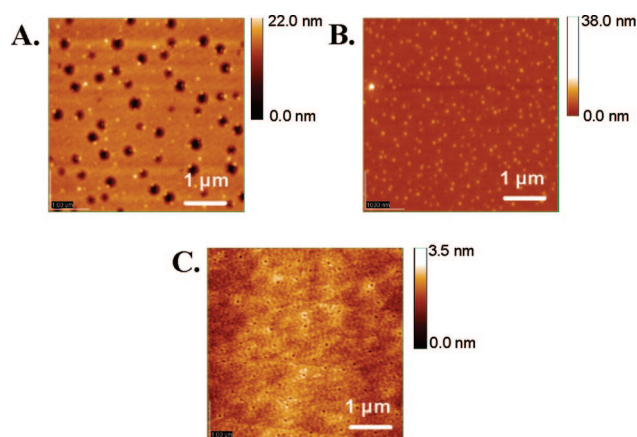
(23) (a) Fritz, S. E.; Kelley, T. W.; Frisbie, C. D. *J. Phys. Chem. B* **2005**, *109*, 10574–10577. (b) Knipp, D.; Street, R. A.; Volkel, A. R. *Appl. Phys. Lett.* **2003**, *82*, 3907–3909.



**Table 2.** PVP-C<sub>6</sub>OAc Film Deposition Conditions<sup>a</sup>

spin-coating solvent (2 mL)	PVP/C <sub>6</sub> OAc ratio (mg/mg)	D	ρ	C <sub>i</sub> <sup>b</sup>
THF	4:8	18	3.0~3.5	260
	4:6	17	2.0~2.5	270
	4:4	14	2.0~2.5	330
dioxane	4:0	22	~0.6	195
	4:8	15	4.0~4.5	310
	4:6	13	1.0~1.5	340
	4:4	10	1.0~1.5	365
EtOAc	4:0	21	~0.6	200
	4:8	17	0.4~0.5	270
	4:6	13	0.3~0.4	345
	4:4	12	0.3~0.4	350
	4:0	20	0.3~0.4	220

<sup>a</sup> Solvent, polymer/crosslinker ratio, film thickness (*D*, nm), RMS roughness ( $\rho$ , nm), and areal capacitance values (*C<sub>i</sub>*, nF cm<sup>-2</sup>).  
<sup>b</sup> Measured in an MIS structure.

**Figure 5.** AFM images of PVP-C<sub>6</sub>OAc (4:6)-based CPB dielectric films deposited from (A) THF, (B) dioxane, and (C) EtOAc.

roughness = 0.3–0.4 nm). Figure 5 shows tapping mode AFM images of spin-coated PVP-C<sub>6</sub>OAc films deposited from THF, dioxane, and EtOAc. Clearly, films fabricated from THF and dioxane afford relatively rough surface morphologies having either pinholes (THF) or small cross-linked particles (dioxane), respectively. Small pinholes are also observed for films fabricated from EtOAc, but possibly due to the small depths (<1 nm), they do not affect the dielectric properties of the films.

Table 3 summarizes optimized conditions (solvent and polymer/cross-linker ratio) for thin (<20 nm) CPB dielectric films fabricated with the various cross-linkers. Here, and for the following studies (vide infra), dielectric film quality was rated from excellent to poor based on the film morphological (roughness) characteristics as well as the dielectric response (leakage current density and breakdown characteristics). Except for films fabricated with C<sub>6</sub>OMe, all of the new cross-linkers afford robust CPB dielectric films. After curing at ~110 °C, these films are completely insoluble in the mother solvent. Because of the very low cross-linking reactivity of C<sub>6</sub>OMe among all of the cross-linkers investigated, robust CPB films using C<sub>6</sub>OMe are probably formed only when cross-linking is carried out in the presence of a Sn or Ti catalyst.<sup>24</sup> However, in this study, cross-linking catalysts were not employed because of their deleterious effect on leakage current.

It is found that optimized polymer/cross-linker weight ratios vary somewhat with the cross-linker. However, for all cross-linkers, the estimated optimum PVP hydroxyl group (–OH): cross-linker molar ratios are ~3:1. THF, dioxane, and EtOAc were used for solvent optimization, with EtOAc affording the smoothest optimized CPB dielectric films for all cross-linkers except C<sub>6</sub>Cl. Even though all the optimized CPB dielectric films afford rather smooth morphologies (rms roughness <1 nm) when an optimized solvent and polymer/cross-linker ratio is employed, there are still significant rms roughness variations.

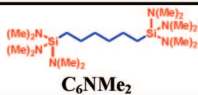
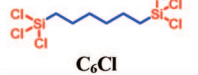
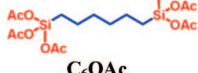

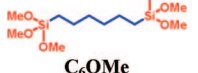
C<sub>6</sub>NMe<sub>2</sub> ( $\rho$  = 0.7–0.8 nm) and C<sub>6</sub>Cl ( $\rho$  = 0.5–0.6 nm), with the most reactive silane groups afford rougher morphologies compared to moderately reactive C<sub>6</sub>OAc ( $\rho$  = 0.3–0.4 nm) and EGOAc ( $\rho$  = 0.2–0.3 nm). These CPB morphological variations with the cross-linker type correlate with the differing OFET performance metrics observed for both p- and n-type semiconductors (vide infra). Similarly, the different cross-linkers afford CPB films with differing electrical properties. Figure 6 presents leakage current density data for various optimized CPB dielectric films. As shown, the C<sub>6</sub>OAc- and EGOAc-based CPB films afford slightly lower leakage current densities ( $J$  = 2–20 × 10<sup>-8</sup> A/cm<sup>2</sup> at 2.0 MV/cm) compared to films prepared with C<sub>6</sub>Cl and C<sub>6</sub>NMe<sub>2</sub> cross-linkers ( $J$  = 8–80 × 10<sup>-8</sup> A/cm<sup>2</sup> at 2.0 MV/cm). As expected, C<sub>6</sub>OMe affords far more leaky films ( $J$  > 1 × 10<sup>-5</sup> A/cm<sup>2</sup> at 2.0 MV/cm). All of the spin-coated thin CPB films except the ones fabricated with C<sub>6</sub>OMe afford breakdown fields between 3–6 MV/cm, independent of the cross-linker (Figure 6B). The areal capacitance values for spin-coated thin and thick CPB films (vide infra) were measured as a function of frequency (*C<sub>i</sub>*-*f*, 1–10<sup>3</sup> kHz) and voltage (*C<sub>i</sub>*-*V*) on metal-insulator-semiconductor (MIS, M = Au, S = n<sup>+</sup>-Si) structures. Capacitance values of CPB films fabricated using C<sub>6</sub>OMe as the cross-linker cannot be measured because of the large leakage currents. Representative *C<sub>i</sub>*-*f* plots are shown in Figure 6C, with the data (Table 3) demonstrating that spin-coated thin CPB films afford large areal capacitance values (300–350 nFcm<sup>-2</sup> at 10 kHz). The formal dielectric constants calculated from the capacitance values using eq 2, are 5.1–5.7 (not shown), which are reasonable considering that the reported dielectric constants of PVP and cross-linked PVP dielectric films are 3.6–6.1.<sup>12,20,25</sup>

**b. Spin-Coated Thick (50–300 nm) CPB Films.** To assess how the different cross-linker reactivities affect the CPB dielectric property transition from thin to thicker films, similar film optimizations based on the aforementioned cross-linking conditions for C<sub>6</sub>Cl, EGOAc, and C<sub>6</sub>NMe<sub>2</sub>, were performed for relatively thick CPB films (50–300 nm) on Si, Al/PEN, and ITO/Mylar substrates. C<sub>6</sub>OMe was not studied because of the poor performance of the corresponding thin CPB films whereas, among the silyl acetates, C<sub>6</sub>OAc-based films exhibit characteristics similar to those of EGOAc (vide infra). Table 4 collects the optimized cross-linking conditions and electrical data for the thick CPB films on Si substrates. Except for C<sub>6</sub>NMe<sub>2</sub>, thick CPB films require different solvents to afford optimally smooth morphologies compared to the corresponding thin films. Furthermore, spin-coated film morphologies depend on the polymer/cross-linker ratio, reagent solubility, solvent volatility/boiling

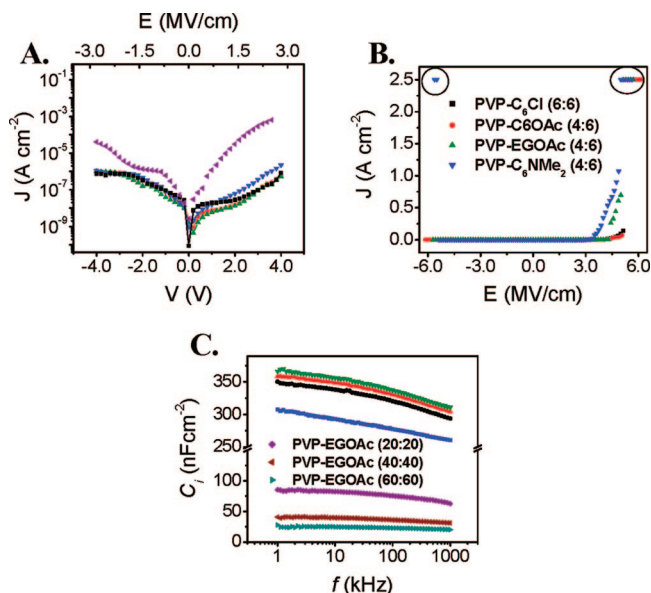
(24) (a) Palmlof, M.; Hjertberg, T. *J. Appl. Polym. Sci.* **1999**, *72*, 521–528. (b) Hjertberg, T.; Palmlof, M.; Sultan, B.-A. *J. Appl. Polym. Sci.* **1991**, *42*, 1185–1192.

(25) (a) Lee, T.-W.; Shin, J. H.; Kang, I.-N.; Lee, S. Y. *Adv. Mater.* **2007**, *19*, 2702–2706. (b) Halik, M.; Klauk, H.; Zschieschang, U.; Kriem, T.; Schmid, G.; Radlik, W.; Wussow, K. *Appl. Phys. Lett.* **2002**, *81*, 289–291. (c) Ullmann, A.; Ficker, J.; Fix, W.; Rost, H.; Clemens, W.; McCulloch, I.; Giles, M. *Mater. Res. Soc. Proc.* **2001**, *665*, C7.5.1–6.

**Table 3.** Spin-Coated CPB Thin Film (<20 nm) Deposition Conditions<sup>a</sup>

crosslinker	ratio (mg:mg)	solvent (2 mL)	quality <sup>b</sup>	<i>D</i>	$\rho$	<i>C<sub>i</sub></i>	<i>J</i>
 C <sub>6</sub> NMe <sub>2</sub>	4:6	THF	G		1–1.5		
		Dioxane	P		>2		
		EtOAc	E	17	0.7–0.8	300	~8 × 10 <sup>-7</sup>
 C <sub>6</sub> Cl	6:6	THF	P		2–3		
		Dioxane	E	14	0.5–0.6	340	8–70 × 10 <sup>-8</sup>
		EtOAc	P		>3		
 C <sub>6</sub> OAc	4:6	THF	P		~2		
		Dioxane	G		1–1.5		
 EGOAc	4:6	THF	P		~2		
		Dioxane	G		1–1.5		
		EtOAc	E	14	0.2–0.3	350	2–10 × 10 <sup>-8</sup>
 C <sub>6</sub> OMe	4:4	THF	P		~1		
		Dioxane	P		>2		
		EtOAc	P	15	0.3–0.4	-	>1 × 10 <sup>-5</sup>

<sup>a</sup> Polymer:crosslinker ratio (mg:mg), solvent, film quality, film thickness (*D*, nm), RMS roughness ( $\rho$ , nm), areal capacitance value (*C<sub>i</sub>*, nF cm<sup>-2</sup>), and leakage current density (*J*, A/cm<sup>2</sup>) at a measurement electric field of 2.0 MV/cm. Films were fabricated on n<sup>+</sup>-Si substrates. <sup>b</sup> Film morphological quality rated as E (excellent), G (good), or P (poor). See text for explanation of terminology.



**Figure 6.** Electrical properties of spin-coated thin CPB films fabricated with various cross-linkers (polymer-cross-linker ratios are as given in Table 3; C<sub>6</sub>NMe<sub>2</sub> = blue, C<sub>6</sub>Cl = black, C<sub>6</sub>OAc = red, EGOAc = green, C<sub>6</sub>OMe = purple). (A) Leakage current density vs voltage plot. (B) Leakage current density vs electric field plot. Circled data indicate the region of breakdown. (C) Capacitance–frequency plots (1–10<sup>3</sup> kHz; film deposition conditions are given in Tables 3 and 4) for ultrathin (top) and thick (bottom) spin-coated CPB films.

point, and film spinning rate. Therefore, different solvents afford films having different qualities depending on the combination of spin-coating conditions and polymer-cross-linker reactivity.<sup>26</sup> Similar to the thin CPB films, films fabricated using moderately reactive EGOAc afford the smoothest film morphologies and superior dielectric response. Thick CPB films fabricated with C<sub>6</sub>Cl and C<sub>6</sub>NMe<sub>2</sub> afford ~10× greater leakage current densities (~1 × 10<sup>-6</sup> A/cm<sup>2</sup>) than those fabricated with EGOAc (~1 ×

10<sup>-7</sup> A/cm<sup>2</sup>) at a measurement electric field of 2.0 MV/cm and have lower breakdown fields,  $E = +4.0$  to  $-4.0$  MV/cm (Figure 7). EGOAc-based CPB films also afford smoother surfaces with an rms roughness of 0.2–0.3 nm versus C<sub>6</sub>Cl (0.3–0.4 nm) or C<sub>6</sub>NMe<sub>2</sub> (2–3 nm)-based films. Note that even the CPB films fabricated with C<sub>6</sub>Cl are relatively smooth, but only over small areas since the overall film quality is poor compared to those fabricated from EGOAc (Supporting Information, Figure S1). Depending on the film thickness, spin-coated thick CPB films exhibit areal capacitance values of 18–82 nF cm<sup>-2</sup> (at 10 kHz; Figure 6C, Table 4). Similar to the case of the spin-coated thin films, the formal dielectric constants calculated from capacitance values for spin-coated thick CPB films using eq 2, are reasonable (4.7–6.2) considering the literature values.<sup>12,20,25</sup>

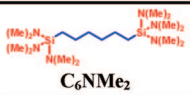
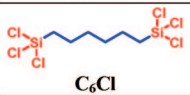

To investigate the compatibility of CPB films with flexible substrates, thick CPB films were also fabricated on flexible Al/PEN and ITO/Mylar substrates using EGOAc as the cross-linker. Table 5 collects the optimized conditions and electrical properties of spin-coated thick CPB dielectric films on these substrates. Compared to the films fabricated on n<sup>+</sup>-Si substrates, the CPB dielectric films fabricated on Al/PEN or ITO/Mylar exhibit slightly rougher surfaces ( $\rho = 0.5$ –0.7 nm) and somewhat greater leakage current densities (~1 × 10<sup>-6</sup> A/cm<sup>2</sup>) at a measurement electric field of 2.0 MV/cm (Figures S2 and S3). Note that the n<sup>+</sup>-Si substrates are far smoother than Al/PEN and ITO/Mylar, with the latter two substrates affording greater CPB roughness.

**c. Printed CPB Films.** Dielectric films were printed on Al/PEN or ITO/Mylar substrates using EGOAc as the cross-linker, which afforded the best dielectric performance among the cross-linking reagents investigated. Printed films using C<sub>6</sub>OAc afford comparable dielectric properties to those based on EGOAc (Table S1, Figure S4). Similar to the optimization process carried out for the spin-coated CPB films, experiments were performed to identify the optimum printing solvent for a given polymer: cross-linker precursor composition and the optimum polymer: cross-linker ratio for a given solvent (Table 6). For a specific PVP/EGOAc concentration ratio (100 mg:50 mg in 0.4 mL

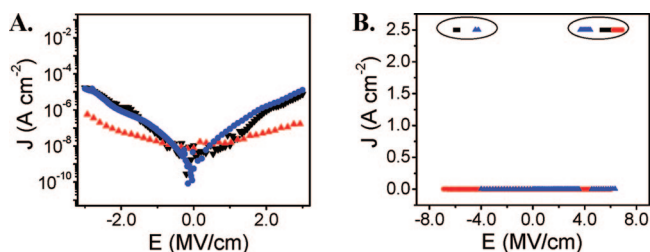
(26) Norrman, K.; Ghanbari-Siahkali, A.; Larsen, N. B. *Annu. Rep. Prog. Chem., Sect. C* **2005**, *101*, 174–201.



**Table 4.** Spin-Coated Thick CPB Film Deposition Conditions and Film Properties<sup>a</sup>

crosslinker	reagent ratio (mg:mg)	solvent (2 mL)	quality <sup>b</sup>	<i>D</i>	$\rho$	<i>C<sub>i</sub></i>	<i>J</i>			
 C <sub>6</sub> NMe <sub>2</sub>	40:40	THF	P		>3					
		Dioxane	P		>2					
		EtOAc	G	90	2–3	55	~1 × 10 <sup>-6</sup>			
 C <sub>6</sub> Cl	40:40	THF	G	155	0.3–0.4	28	~1 × 10 <sup>-6</sup>			
		Dioxane	P		1–1.5					
		EtOAc	P		>3					
 EGOAc	40:40	Dioxane	E							
				20:20	THF	P		>3		
				40:40			50		82	
				60:60			130	0.2–0.3	40	~1 × 10 <sup>-7</sup>
				80:80			205		25	
	40:40	EtOAc	P		>3					

<sup>a</sup> Polymer:crosslinker ratio (mg:mg), solvent, film quality, film thickness (*D*, nm), RMS roughness ( $\rho$ , nm), areal capacitance value (*C<sub>i</sub>*, nF cm<sup>-2</sup>), and leakage current density at a measurement electric field of 2.0 MV/cm (*J*, A/cm<sup>2</sup>). Films were fabricated on an n<sup>+</sup>-Si substrate. <sup>b</sup> Film morphological quality rated as E (excellent), G (good), or P (poor). See text for explanation of terminology.



**Figure 7.** Electrical properties of spin-coated thick CPB films. (PVP-C<sub>6</sub>Cl (40:40) = black, PVP-EGOAc (40:40) = red, PVP-C<sub>6</sub>NMe<sub>2</sub> (40:40) = blue; solvents are given in Table 4): (A) Leakage current density vs electric field plot; (B) extended leakage current density vs electric field plot. Circled data indicate the region of breakdown.

**Table 5.** Spin-Coated Thick CPB Film Properties for Films Fabricated from PVP-EGOAc in Dioxane (2 mL)<sup>a</sup>

entry	gate	PVP:EGOAc (mg:mg)	<i>D</i>	<i>C<sub>i</sub></i> <sup>b</sup>
1	n <sup>+</sup> -Si	80:80	305	18
2	n <sup>+</sup> -Si	60:60	205	25
3	n <sup>+</sup> -Si	40:40	130	40
4	n <sup>+</sup> -Si	30:30	80	55
5	n <sup>+</sup> -Si	20:20	50	82
6	Al/PEN	80:80	300–310	20
7	Al/PEN	60:60	200–210	27
8	Al/PEN	40:40	125–135	44
9	Al/PEN	30:30	80	58
10	Al/PEN	20:20	50	85
11	ITO/Mylar	80:80	300–310	22
12	ITO/Mylar	60:60	200–210	27
13	ITO/Mylar	40:40	125–135	49
14	ITO/Mylar	30:30	80	58
15	ITO/Mylar	20:20	50	87

<sup>a</sup> Gate dielectric, polymer:crosslinker ratio (mg:mg), film thickness (*D*, nm), and areal capacitance value (*C<sub>i</sub>*, nF/cm<sup>2</sup>). <sup>b</sup> Measured in a MIS/MIM structure.

solvent), films fabricated with EtOAc as the solvent afford by far the most impressive dielectric characteristics. Similarly, the optimum polymer/cross-linker concentration ratios were determined to be PVP:cross-linker at ~100 mg:50 mg in 0.4 mL solvent, using EtOAc as the solvent and using the printing parameters provided in the Experimental Section (see Supporting Information). Gravure-printed CPB films fabricated under optimum printing conditions (solvent, polymer/cross-linker ratio)


exhibit thicknesses of 450–550 nm and areal capacitance values of 5.5–7.5 nF cm<sup>-2</sup>. Note that the gravure-printed films afford somewhat “wavy” surface features typical of the particular engraved printing cylinder used in this study. Furthermore, the gravure-printed CPB films afford very good electrical properties with low leakage current densities of ~1 × 10<sup>-7</sup> A/cm<sup>2</sup> at 2.0 MV/cm (Figure 8).

Figure S4 shows AFM images of CPB dielectric films printed from optimized precursor compositions. These images demonstrate that the optimized printed dielectric films exhibit very smooth surfaces (rms roughness = 0.3–0.4 nm). Similarly, Figure S5 shows optical images of gravure-printed dielectric films fabricated using C<sub>6</sub>Cl and EGOAc cross-linkers, demonstrating that cross-linker design is essential to achieving acceptable printed dielectrics. Furthermore, the data of Table 6 clearly demonstrate that identifying the optimal composition of the dielectric precursor formulations (type of polymer, solvent, as well as polymer/cross-linker concentration ratio) is critical to achieving optimally pinhole- and defect-free dielectric films.

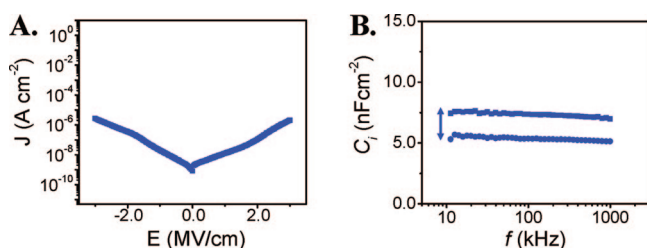
**OFET Fabrication and Performance.** Top-contact FETs were fabricated using spin-coated and gravure-printed CPB films as the gate dielectrics on n<sup>+</sup>-Si, Al/PEN, or ITO/Mylar gate substrates. Both p-type (**P5**) and n-type (**DFHCO-4T**) organic semiconductors were employed (Figure 2). FET devices were fabricated by spin-coating or printing PVP-cross-linker mixture solutions, curing in a vacuum oven at 110 °C, followed by semiconductor and Au source-drain contact vapor deposition. All OFET devices were characterized under vacuum. Transfer characteristics of the devices were measured in the saturation regime ( $V_{DS} \geq V_G - V_T$ ), and representative transfer plots are shown in Figures 9–11. Tables 7 and 8 collect the OFET performance parameters, carrier mobilities in the saturation regime ( $\mu_{sat}$ ), and current on/off ratios ( $I_{on}/I_{off}$ ).  $\mu_{sat}$  is calculated from the slope of the linear part of the  $I_{DS}^{1/2} - V_G$  plot by fitting the data to  $\mu_{sat} = (2I_{DS}L)/[WC_i(V_G - V_T)^2]$ .<sup>11</sup>

**a. OFETs Fabricated with Spin-Coated CPB Films.** Figures 9 and 10 show representative transfer and output plots for **P5** and **DFHCO-4T** transistors fabricated with spin-coated CPB films as gate dielectrics. As shown in Figure 9, devices fabricated with thin CPB dielectric films function at low operating voltages ( $\pm 3.0$  V) as a consequence of the large areal

**Table 6.** Gravure-Printed CPB Dielectric Film Fabrication Conditions and Film Properties<sup>a</sup>

crosslinker	ratio (mg:mg)	solvent (0.4 mL)	quality <sup>b</sup>	<i>D</i>	$\rho$	<i>C<sub>i</sub></i>	<i>J</i>
 <b>EGOAc</b>	100:50	THF	G	450–550	0.3–0.4	5.5–7.5	$\sim 1 \times 10^{-7}$
		Dioxane	G				
		EtOAc	E				
		CP	P				
		EtOH	G				
 <b>EGOAc</b>	100:20	MeOH	P	450–550	0.3–0.4	5.5–7.5	$\sim 1 \times 10^{-7}$
		EtOAc	E				
		CP	P				
		EtOH	G				
		MeOH	P				
		EtOAc	E				
		CP	P				

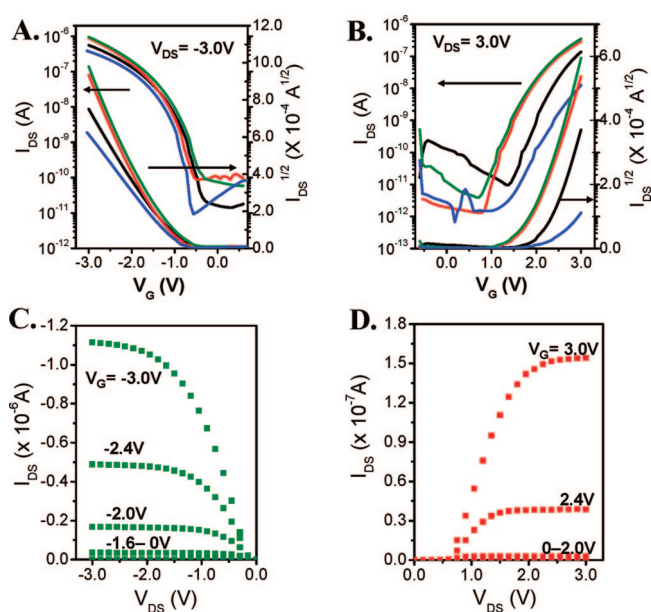
<sup>a</sup> Polymer:crosslinker ratio (mg:mg), solvent, film quality, film thickness (*D*, nm), RMS roughness ( $\rho$ , nm), areal capacitance value (*C<sub>i</sub>*, nF cm<sup>-2</sup>), and leakage current density at a measurement electric field of 2.0 MV/cm (*J*, A/cm<sup>2</sup>). Films were fabricated on Al/PEN or ITO/Mylar substrate. <sup>b</sup> Film morphological quality rated as E (excellent), G (good), or P (poor). See text for explanation of terminology.



**Figure 8.** Electrical properties of gravure-printed CPB films: (A) leakage current density vs electric field plot; (B) capacitance–frequency plots (10–10<sup>3</sup> kHz) for gravure-printed CPB films. (PVP:EGOAc (100:50), polymer (mg):cross-linker (mg) in 0.4 mL EtOAc). Arrow indicates an areal capacitance range of 5.5–7.5 nF cm<sup>-2</sup>.

capacitance values (300–350 nF/cm<sup>2</sup>). Device operating voltages increase as the gate dielectric film thicknesses increase (as the capacitance values decrease) from 3.0 V (PVP-EGOAc 4:6, 14 nm thickness) to 60 V (PVP-EGOAc 80:80, 305 nm thickness). These OFETs exhibit mobilities of 0.12–0.49 and 0.02–0.52 cm<sup>2</sup>/Vs for **P5** and **DFHCO-4T**, respectively—comparable to those based on 300 nm thick SiO<sub>2</sub> dielectrics (Table 7). Note that because of the optimized gate dielectric surface morphologies, **P5** devices afford higher mobilities than those achieved with first-generation CPBs (0.10 cm<sup>2</sup>/Vs).<sup>12</sup> These results demonstrate the importance of cross-linker and solvent optimization. For devices fabricated with all of the present dielectric films,  $I_{\text{on}}/I_{\text{off}} = 10^4$ – $10^6$ . The high contact resistance observed for the output characteristics of **DFHCO-4T**-based devices (Figures 9D and 10F) can be attributed to the high injection barrier between the **DFHCO-4T** LUMO (3.96 eV)<sup>21</sup> and the Au work function (5.1 eV). OFETs fabricated on flexible Al/PEN substrates afford somewhat lower performance compared to those on Si substrates with  $\mu_{\text{sat}} = 0.26$ – $0.34$  cm<sup>2</sup>/Vs and  $I_{\text{on}}/I_{\text{off}} = \sim 10^5$  (Table 7, Figure S6).

**b. OFETs Based on Printed CPB Films.** Similar to the spin-coated films, gravure-printed CPB films on Al/PEN or ITO/Mylar substrates were also employed as dielectrics for OFET fabrication. Table 8 summarizes OFET performance data for the two different semiconductors (**P5** and **DFHCO-4T**) on various gravure-printed CPB films. In all cases, the devices are FET-active and the computed carrier mobilities are comparable to those on 300 nm-thick SiO<sub>2</sub> substrates (Table 7). **P5** and **DFHCO-4T** transistors fabricated on the printed dielectric are



**Figure 9.** Performance of OFET devices fabricated with spin-coated thin CPB films using various cross-linkers (polymer/cross-linker ratios are as given in Table 3: C<sub>6</sub>NMe<sub>2</sub> = blue, C<sub>6</sub>Cl = black, C<sub>6</sub>OAc = red, EGOAc = green). OFET transfer characteristics for (A) **P5**, (B) **DFHCO-4T**; OFET output characteristics for (C) **P5** on PVP-EGOAc (4:6) and (D) **DFHCO-4T** on PVP-C<sub>6</sub>OAc (4:6). The channel width and length are 500 and 100  $\mu\text{m}$  (for **P5**) or 1000 and 100  $\mu\text{m}$  (for **DFHCO-4T**), respectively.

found to exhibit good device performance metrics, affording carrier mobilities of 0.3–0.9 cm<sup>2</sup>/Vs. Figure 11 shows representative transfer and output plots of pentacene film OFET devices fabricated on one of the gravure-printed PVP-EGOAc (100:50) formulations. Note also that the printed OFET devices exhibit excellent mechanical flexibility (Figure 12).

## Discussion

**CPB Morphology versus FET Response Characteristics.** All cross-linking reactions employed in this study yield robust, insoluble CPB siloxane networks (Scheme 1), exhibiting identical chemical composition. The only major differences between the various spin-coated thin CPB films are the details of film morphologies (roughness), originating from the differing cross-

**Table 7.** Carrier Mobility ( $\mu_{\text{sat}}$ ,  $\text{cm}^2/\text{Vs}$ ) and Current On/Off Ratio ( $I_{\text{on}}/I_{\text{off}}$ ) Data for OFET Devices Fabricated Using **P5** and **DFHCO-4T** as the p- and n-type Organic Semiconductor on Various CPBs<sup>a</sup>

substrate	cross-linker	ratio	P5		DFHCO-4T	
			$\mu_{\text{sat}}^b$	$I_{\text{on}}/I_{\text{off}}$	$\mu_{\text{sat}}^b$	$I_{\text{on}}/I_{\text{off}}$
n <sup>+</sup> -Si	C <sub>6</sub> NMe <sub>2</sub> C <sub>6</sub> Cl C <sub>6</sub> OAc EGOAc	4:6	0.12	10 <sup>5</sup>	0.02	10 <sup>5</sup>
		6:6	0.18	10 <sup>5</sup>	0.11	10 <sup>4</sup>
		4:6	0.35	10 <sup>4</sup>	0.12	10 <sup>6</sup>
		4:6	0.37	10 <sup>4</sup>	0.16	10 <sup>5</sup>
		20:20	0.40	10 <sup>5</sup>	0.44	10 <sup>6</sup>
		40:40	0.34	10 <sup>6</sup>	0.43	10 <sup>6</sup>
Al/PEN	EGOAc	60:60	0.43	10 <sup>6</sup>	0.47	10 <sup>5</sup>
		80:80	0.49	10 <sup>7</sup>	0.52	10 <sup>5</sup>
		20:20	0.30	10 <sup>5</sup>		
		40:40	0.34	10 <sup>5</sup>		
		60:60	0.26	10 <sup>5</sup>		
n <sup>+</sup> -Si	first generation CPB <sup>c</sup>		0.10	10 <sup>4</sup>		
n <sup>+</sup> -Si	300 nm SiO <sub>2</sub> <sup>d</sup>		0.39	10 <sup>5</sup>	0.37	10 <sup>7</sup>

<sup>a</sup> Gate dielectric films were spin-coated on n<sup>+</sup>-Si or Al/PEN substrates. <sup>b</sup> Calculated for the charge carrier concentration  $n_Q = C_i V_G / e = 5-6 \times 10^{12} \text{ cm}^{-2}$ . <sup>c</sup> From previous study (ref 11). <sup>d</sup> Data are for 300 nm-thick SiO<sub>2</sub>/Si devices with pentacene films grown under the same conditions as for other CPB films.

**Table 8.** Carrier Mobility ( $\mu_{\text{sat}}$ ,  $\text{cm}^2/\text{Vs}$ ) and Current On/Off Ratio ( $I_{\text{on}}/I_{\text{off}}$ ) for OFET Devices Fabricated with Various Gravure-Printed CPB Films on Al/PEN and ITO/Mylar substrates

substrate	PVP (mg):EGOAc (mg) (0.4 mL EtOAc)	semiconductor	$\mu_{\text{sat}}$	$I_{\text{on}}/I_{\text{off}}$
Al/PEN	100:50	<b>P5</b>	0.29–0.76	10 <sup>6</sup>
ITO/Mylar	100:50	<b>P5</b>	0.44–0.85	10 <sup>4</sup>
Al/PEN	100:50	<b>DFHCO-4T</b>	0.58–0.86	10 <sup>5</sup>
ITO/Mylar	100:50	<b>DFHCO-4T</b>	0.38–0.60	10 <sup>6</sup>

linker reactivities. Note that as a consequence of the uniformly low leakage current densities ( $<1 \times 10^{-6} \text{ A/cm}^2$  at 2.0 MV/cm) for all spin-coated CPB films, the differing dielectric properties of the various films have little effect on OFET responses at relatively low device operating voltages. However, the OFET performance trends measured for devices fabricated with the spin-coated CPB films are rather sensitive to the dielectric film morphologies. For spin-coated thin CPB films, the **P5** FET devices fabricated with the EGOAc-based dielectrics, having the smoothest film morphology, exhibit the largest carrier mobility,  $\sim 0.40 \text{ cm}^2/\text{Vs}$ , among all cross-linkers examined, followed by C<sub>6</sub>OAc ( $\mu_{\text{sat}} = 0.35 \text{ cm}^2/\text{Vs}$ ), C<sub>6</sub>Cl ( $\mu_{\text{sat}} = 0.18 \text{ cm}^2/\text{Vs}$ ), and C<sub>6</sub>NMe<sub>2</sub> ( $\mu_{\text{sat}} = 0.12 \text{ cm}^2/\text{Vs}$ ). Interestingly, a similar dielectric morphology-mobility trend is observed for the n-type semiconductor **DFHCO-4T**. Since OFET charge transport is confined to the nanoscopic region at the semiconductor/dielectric interface, the smoothness of the dielectric film surface is clearly a prerequisite here to optimizing OFET performance. In the case of pentacene FETs, several groups<sup>23,27</sup> have reported that rough gate dielectric surfaces induce the growth of smaller pentacene grains rather than with very smooth substrates, and that roughness leads to poor FET response. Grain boundaries between semiconductor crystallites are thought to function as interfacial charge trapping sites which disrupt carrier drift.<sup>28</sup> Pentacene films grown on smoother CPB films fabricated

with C<sub>6</sub>OAc and EGOAc afford large, dendritic grains ( $>2 \mu\text{m}$ ), whereas far smaller grains ( $<0.4 \mu\text{m}$ ) are observed on C<sub>6</sub>Cl- and C<sub>6</sub>NMe<sub>2</sub>-based dielectric films (Figure 13). Note that **P5** films deposited on spin-coated thick EGOAc-based CPB films ( $D = 50-305 \text{ nm}$ ) afford large, dendritic grains, independent of the dielectric film thickness. Because of the smooth film morphology, these **P5** FETs exhibit similar carrier mobilities (Table 7, Figure 13).

The high carrier mobility and current on/off ratio achieved with **P5** and **DFHCO-4T** FETs based on spin-coated and gravure-printed CPB films also imply very good semiconductor film crystallinity. Figures 14 and S7 show XRD  $\theta-2\theta$  scans of 50 nm-thick **P5** and **DFHCO-4T** films deposited on spin-coated and gravure-printed CPB films. Indeed, all of the XRD spectra exhibit sharp, multiple Bragg reflections demonstrating a large degree of texture, with those fabricated on smoother dielectric surfaces exhibiting far larger intensities. It is well-known that rough surfaces disrupt the growth of highly textured pentacene grains.<sup>27a,29</sup> A similar effect of the dielectric morphology on semiconductor film growth is observed for the first time here for **DFHCO-4T**.

**Humidity-Dependent Electrical Properties.** Previous studies showed that the performance of OFETs based on PVP or cross-linked PVP gate dielectric films are significantly affected by surface polarization at the semiconductor/dielectric interface induced by absorbed water molecules in the dielectric.<sup>30</sup> Thus, OFETs fabricated with the present CPB materials were characterized both in vacuo and in humidity-controlled environments. To provide comprehensive characterization of the CPB materials, humidity-dependent dielectric properties and the corresponding **P5** FET performance were investigated for the different CPB compositions. For this study, only CPB films affording excellent surface characteristics such as spin-coated PVP-EGOAc (4:6,  $D = 14 \text{ nm}$ ), PVP-EGOAc (40:40,  $D = 130 \text{ nm}$ ), and PVP-EGOAc (80:80,  $D = 305 \text{ nm}$ ) and printed PVP-EGOAc (100:50,  $D = 450-550 \text{ nm}$ ; as given in Tables 3, 4, and 6) were employed. Figure 15 shows measured leakage current densities plotted versus electric field under various humidity levels (from vacuum to relative humidity (RH) = 36%). In all cases, the leakage current density of these MIS/MIM capacitors increases when the RH is increased. In the case of the spin-coated thin CPB films (PVP-EGOAc 4:6) with the lowest PVP content, the leakage current densities at high RH ( $>26\%$ ) increase about an order of magnitude at most, compared with those measured at low RH ( $<8\%$ ). As the PVP content increases, going from thin to thick spin-coated films to printed CPB films, the leakage current densities become more sensitive to moisture. Thus, for spin-coated thick CPB films,  $J$  increases slightly at RH = 8% compared to vacuum, and to  $>10\times$  at RH  $> 26\%$ . Furthermore, printed CPB films having the greatest PVP content afford  $J \approx 10\times$  greater at RH = 8%, and  $J > 100\times$  greater at RH  $> 26\%$ .

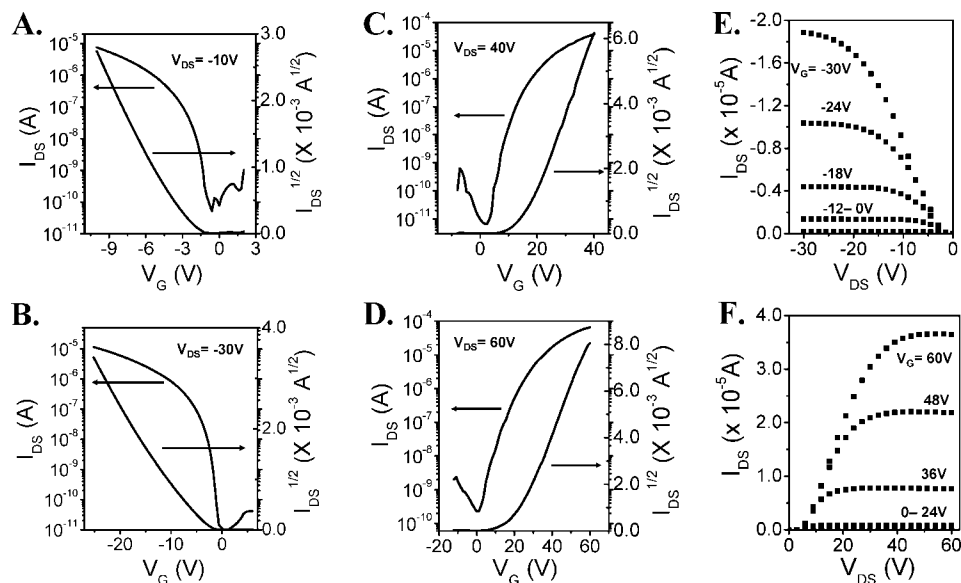
**P5** OFETs fabricated with the present CPB films exhibit similar behavior when evaluated under conditions of differing humidity. Spin-coated thin CPB films (PVP-EGOAc 4:6) are least affected by the various humidity levels. For these films, field-effect mobilities afford little variation between vacuum and RH = 26%, and a slight increase at RH = 36% (not shown).

(27) (a) Kim, C.; Facchetti, A.; Marks, T. J. *Adv. Mater.* **2007**, *19*, 2561–2566. (b) Stuedel, S.; de Vusser, S.; de Jonge, S.; Janssen, D.; Verlaak, S.; Senoe, P.; Heremans, J. *Appl. Phys. Lett.* **2004**, *85*, 4400–4402. (28) Bolognesi, A.; Berliocchi, M.; Manenti, M.; Carlo, A. D.; Lugli, P.; Lmimouni, K.; Dufour, C. *IEEE Trans. Electron Devices* **2004**, *51*, 1997–2003.

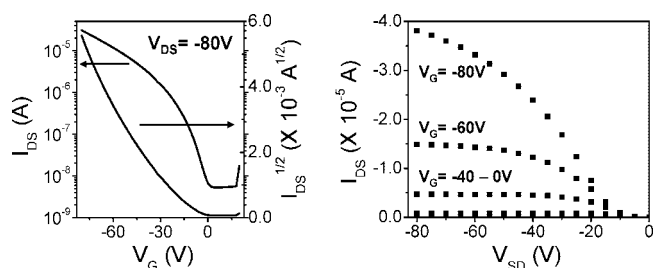
(29) Kim, C.; Facchetti, A.; Marks, T. J. *Science* **2007**, *318*, 76–80.

(30) (a) Jung, T.; Dodabalapur, A.; Wenz, R.; Mohapatra, S. *Appl. Phys. Lett.* **2005**, *87*, 182109/1–3. (b) Bäcklund, T. G.; Österbacka, R.; Stubb, H.; Bobacka, J.; Ivaska, A. *J. Appl. Phys.* **2005**, *98*, 074504/1–6.

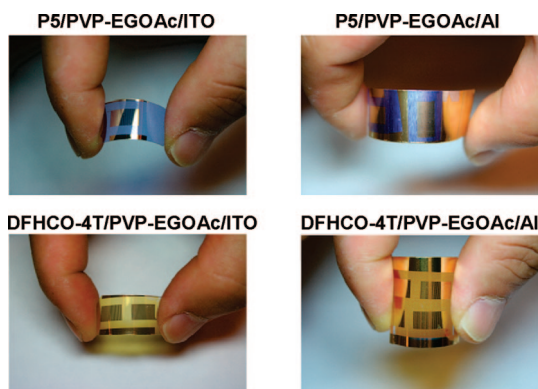




**Figure 10.** Performance of OFET devices fabricated with spin-coated thick CPB films (deposition conditions are as given in Table 4). OFET transfer characteristics for **P5** on (A) PVP-EGOAc (20:20), (B) PVP-EGOAc (40:40) and for **DFHCO-4T** on (C) PVP-EGOAc (60:60), and (D) PVP-EGOAc (80:80). OFET output characteristics for (E) **P5** on PVP-EGOAc (40:40), and (F) **DFHCO-4T** on PVP-EGOAc (80:80). The channel width and length are 500 and 100  $\mu\text{m}$  (for **P5**) or 1000 and 100  $\mu\text{m}$  (for **DFHCO-4T**), respectively.

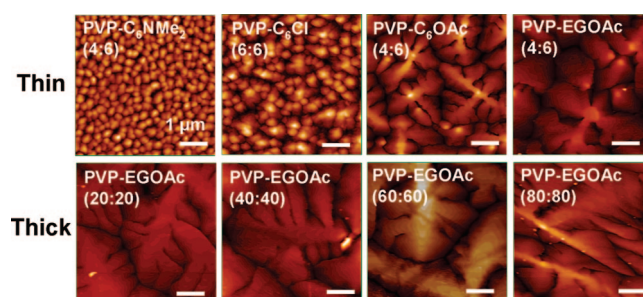


**Figure 11.** Transfer and output characteristics for **P5** OFET devices fabricated on gravure-printed CPB (PVP-EGOAc = 100 mg:50 mg in 0.4 mL EtOAc) dielectric films using ITO/Mylar as the substrate. The channel length and width are 100 and 500  $\mu\text{m}$ , respectively.



**Figure 12.** Photographs of the indicated printed OFETs demonstrating mechanical flexibility.

Figure 16 shows **P5** OFET transfer characteristics for devices fabricated with spin-coated (PVP-EGOAc 40:40) and printed (PVP-EGOAc 100:50) CPB films. For the spin-coated CPB films (Figure 16A,B), the field-effect mobility of **P5** OFETs increases slightly from 0.35 to 0.50  $\text{cm}^2/\text{Vs}$  when the moisture level increases from RH = 0% (vacuum) to RH = 26%. An even greater  $\mu$  of 0.90  $\text{cm}^2/\text{Vs}$  is observed at RH = 36%. The mobility increase at higher moisture levels is even more



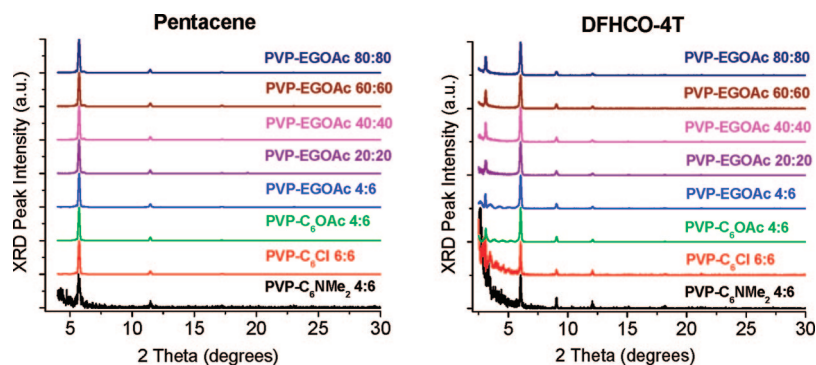
**Figure 13.** AFM images of 50 nm thick pentacene films grown on various spin-coated thin and thick CPB films (PVP (mg)/cross-linker (mg) in 2 mL of solvent as given in Tables 3 and 4). The scale bars indicate 1  $\mu\text{m}$ .

significant for OFET devices based on printed CPB gate dielectric films. Thus, **P5** OFET mobilities increase from 0.36  $\text{cm}^2/\text{Vs}$  under vacuum, to 3.3 at RH = 8%, to 5.3 at RH = 26% and 8.5 at RH = 36%. The increase in source-drain current is attributed to the accumulation/stabilization of extra charge carriers at the semiconductor/dielectric interface induced by the surface polarization from the absorbed moisture in the dielectric film.<sup>30</sup> At high humidities, due to increased gate leakage current, decreased source-drain current is observed at high gate voltages. The previously reported exceptional mobilities (3–5  $\text{cm}^2/\text{Vs}$ ) of **P5** OFET devices using PVP or PVP-like polymers as dielectrics could also be attributed to such effects.<sup>1c,31</sup> Because of an increased source-drain current in the off-state,  $I_{\text{on}}/I_{\text{off}}$  decreases at high RH for all OFET devices examined (Figure 16).

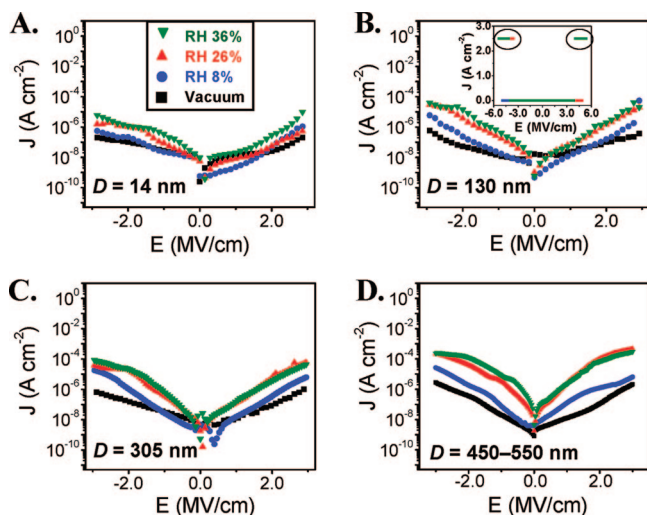
## Conclusions

We have reported newly designed  $\alpha,\omega$ -disilane cross-linkers with tuned reactivity, optimized by an in situ reaction kinetic study. With these new cross-linkers, we have demonstrated that optimization of cross-linking processes with PVP, employing

(31) Lee, S.; Koo, B.; Shin, J.; Lee, E.; Park, H.; Kim, H. *Appl. Phys. Lett.* **2006**, *88*, 162109/1–3.

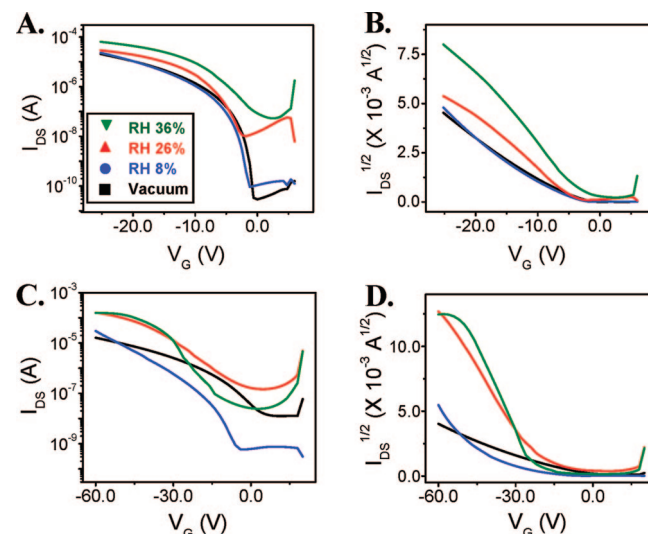


**Figure 14.** The  $\theta$ - $2\theta$  XRD spectra of 50 nm-thick P5 (left) and DFHCO-4T (right) films grown on spin-coated CPB films (PVP/cross-linker ratios are as indicated).



**Figure 15.** Leakage current densities versus electric field of various CPB films measured under different relative humidity (RH) levels (black, vacuum; blue, RH 8%; red, RH 26%; green, RH 36%): (A) spin-coated thin films (PVP-EGOAc, 4:6); (B) spin-coated thick films (PVP-EGOAc 40:40); (inset) expanded leakage current density plot. Circled data indicate the region of breakdown; (C) spin-coated thick films (PVP-EGOAc 80:80). For spin-coated films, PVP (mg)/EGOAc (mg) in 2 mL of dioxane. (D) Printed films (PVP-EGOAc 100:50 on Al/PEN film). For printed films, PVP (mg)/EGOAc (mg) in 0.4 mL of EtOAc.

moderately reactive cross-linkers, appropriate solvent, and appropriate polymer/cross-linker concentration ratios affords robust, adherent, pinhole-free, and smooth gate dielectric materials with tunable thickness and capacitance. These films are readily deposited from solution by spin-coating or gravure printing, adhere strongly to a variety of conducting substrates, and are compatible with p- and n-type organic semiconductors. These results demonstrate that robust, low-leakage polymer dielectric films are accessible and that the FET devices utilizing these polymer dielectrics in solution-processed fabrication methodologies offer attractive opportunities for printing applications. While the hygroscopic nature of PVP to some degree affects electrical properties of the dielectric films and the resultant OFET device performance (depending on the exact film composition), such effects are not in general severely



**Figure 16.** Response of P5 OFET devices fabricated with CPB films under different relative humidity levels (black, vacuum; blue, RH 8%; red, RH 26%; green, RH 36%). Transfer characteristics on spin-coated thick (PVP-EGOAc 40:40) films: (A)  $I_{DS}$  versus  $V_G$ ; (B)  $I_{DS}^{1/2}$  versus  $V_G$ . Transfer characteristics on printed (PVP-EGOAc 100:50 on Al/PEN substrate) films: (C)  $I_{DS}$  versus  $V_G$ ; (D)  $I_{DS}^{1/2}$  versus  $V_G$ . Channel width and length are 1000 and 100  $\mu\text{m}$  (A and B) or 500 and 100  $\mu\text{m}$  (C and D), respectively.  $V_{DS}$  is  $-30$  and  $-80$  V for spin-coated and printed films, respectively.

detrimental to OFET performance and should be suppressable by simple encapsulation procedures.<sup>32</sup> Moisture absorbed in the dielectric film appears to induce additional charge carriers, resulting in increased gate leakage and source-drain current as well as in apparent mobility.

**Acknowledgment.** This contribution is dedicated to the memory of Mr. Hyuk-Jin Choi. This research was supported by ONR (Grant N00014-02-0909) and Polyera Corp. We thank the NSF-MRSEC program through the Northwestern Materials Research Center (Grant DMR-0520513) for providing characterization facilities.

**Supporting Information Available:** Experimental details, optical microscope image, AFM image, XRD, leakage current density, and OTFT device performance data for chosen dielectric materials. This material is available free of charge via the Internet at <http://pubs.acs.org>.

(32) (a) Feili, D.; Schuettler, M.; Doerge, T.; Kammer, S.; Stieglitz, T. *Sensors and Actuators A* **2005**, *120*, 101–109. (b) Kawashima, N.; Nomomoto, K.; Wada, M.; Kasahara, J. *Mater. Res. Soc. Proc.* **2005**, *871*, 11.10.1–6.